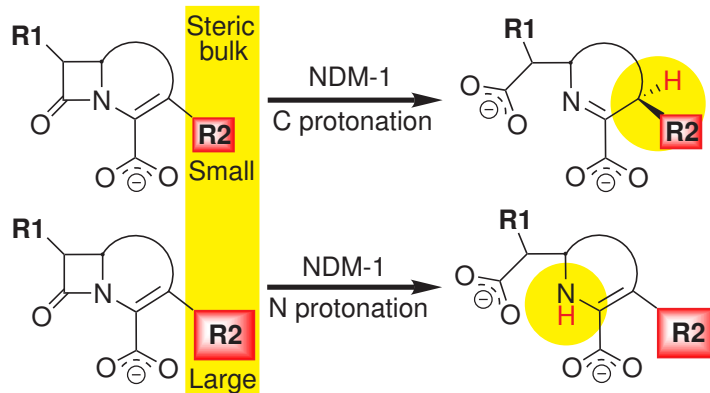


Hydrolysis of Cephalexin and Meropenem by New Delhi Metallo β -Lactamase: Substrate Protonation Mechanism is Drug Dependent

Chandan Kumar Das and Nisanth N. Nair*

Department of Chemistry, Indian Institute Of Technology Kanpur, Kanpur 208016, India

E-mail: nnair@iitk.ac.in



Abstract

Emergence of antibiotic resistance due to New Delhi Metallo β -lactamase (NDM-1) bacterial enzymes is of great concern due to their ability to hydrolyze wide range of antibiotics. Efforts are ongoing to obtain the atomistic details of the hydrolysis mechanism in order to develop novel drugs and inhibitors against NDM-1. Especially, it remains elusive how drug molecules of different family of antibiotics are hydrolyzed by NDM-1 in an efficient manner. Here we report the detailed molecular mechanism of NDM-1 catalyzed hydrolysis of cephalexin, a cephalosporin family drug, and meropenem, a carbapenem family drug. This study employs molecular dynamics (MD) simulations using hybrid quantum mechanical/molecular mechanical (QM/MM) methods at the density functional theory level, based on which reaction pathways and the associated free energies are obtained. We find that the mechanism and the free energy barrier for the ring-opening step are the same for both the drug molecules, while the subsequent protonation step differs. In particular, we observe that the mechanism of the protonation step depends on the R2 group of the drug molecule. Our simulations show that allylic carbon protonation occurs in the case of cephalexin drug molecule where Lys211 is the proton donor and the proton transfer occurs via a water chain formed (only) at the ring-opened intermediate structure. Based on the free energy profiles, the overall kinetics of the drug hydrolysis is discussed. Finally, we show that the proposed mechanisms and free energy profiles could explain various experimental observations.

Introduction

Escalating antimicrobial resistance (AMR) has been realized as a global threat to the public health in the recent times.¹ AMR related death is estimated to be about 700 000 per year and it is predicted to be the biggest devastating problem by 2050 with 10 million deaths per year.² Implementation of effective measures to combat drug resistance shown by bacteria, in particular, development of novel antimicrobial drugs, has to be expedited. One of the ways in which bacteria develop antibiotic resistance is by expressing β -lactamase enzymes, which catalyze the hydrolysis of antibiotic drug molecules in an efficient way. New Delhi Metallo- β -lactamase-1 (NDM-1) is one such enzymes which was identified only in 2009,³ however becoming widely expressed in bacteria causing hospital-acquired and community-acquired infections.⁴ Of great concern, NDM-1 carrying bacteria are known to hydrolyze nearly all the clinically used β -lactam antibiotics including penicillins, cephalosporins and even carbapenems considered as the last resort drugs.⁵⁻⁸ Thus there is an urgent need to develop effective inhibitors for NDM-1 so that life threatening infections due to NDM-1 carrying “superbugs” be cured.

Development of inhibitors is majorly aided by the knowledge of structure and reactivity of the active site. Over the last few decades a number of crystallographic,⁹⁻¹² spectroscopic,¹³⁻²⁴ and computational^{11,25-32} studies have reported which shed light on the molecular structure and catalytic reactions of di-Zn metallo β -lactamases (MBLs), including NDM-1. Active site of NDM-1 has two Zn(II) binding sites bridged with a hydroxide (W1). The Zn1 site is coordinated with His120, His122, and His189, while the Zn2 site is bound to Asp124, Cys208, and His250. The existence of a water molecule bound to Zn2 in the apoenzyme is also debated.³³

Based on the existing studies on NDM-1 and other di-Zn Class B1 MBLs,³³⁻³⁵ the hydrolysis is initialized by the nucleophilic attack (**ES** \rightarrow **EI**) where the bridging hydroxide attacks the β -lactam ring of the drug molecules (see Figure 1). This leads to the intermediate structure **EI** where the β -lactam N of the ring-opened drug molecule is bound to Zn2.

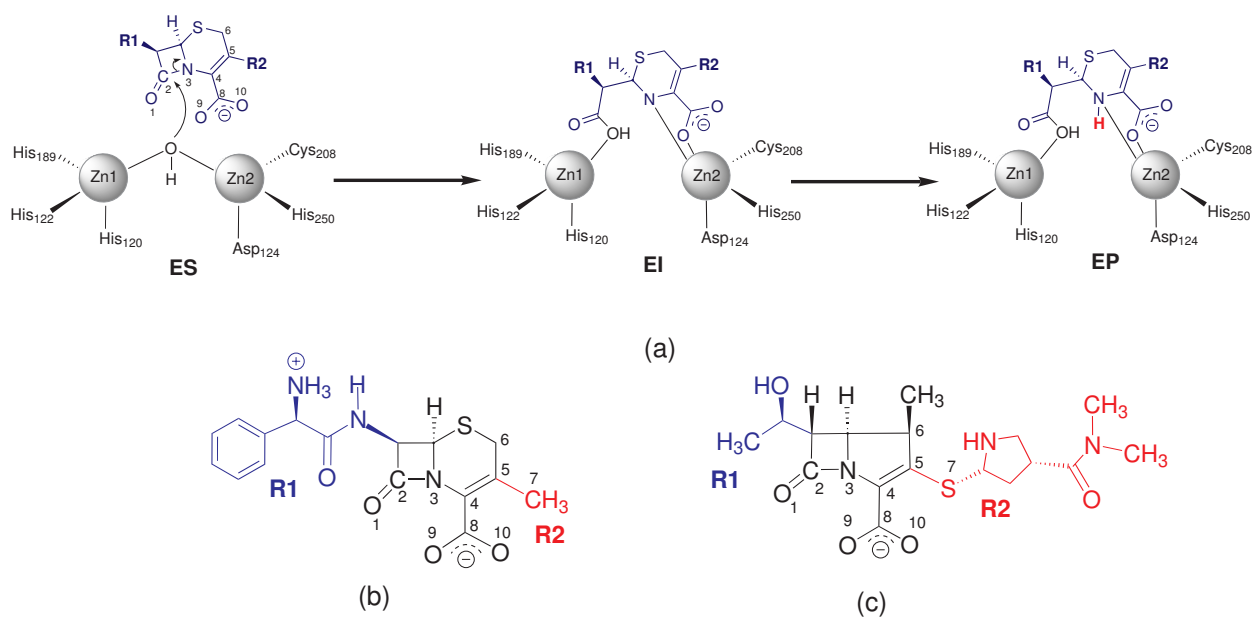


Figure 1: (a) General mechanism of NDM-1 catalyzed β -lactam antibiotic hydrolysis. Chemical structure of cephalexin (b) and meropenem (c). R1 and R2 groups are shown in blue and in red, respectively.

The subsequent step involves a proton transfer to N₃ (or C₅) and is followed by decoordination of the drug from the active site, completing the hydrolysis; see Figure 1 for the atom numbers followed. However, the detailed mechanism of hydrolysis is not fully understood. Mostly, the proton donor has to be identified and the mechanism of proton transfer has to be ascertained. Further, the rate-determining step of the whole process has to be established.

In general, proton transfer to N₃ is anticipated, while C₅ protonation has been also noticed in some experimental studies.^{9,18} A tautomerization where C₄-C₅ double bond is migrated to N₃-C₄ could result in protonation of C₅ instead of N₃, and was noted in the experiments by Tioni et al.¹⁸ while studying the carbapenem hydrolysis by BcII MBL. Protonation of C₅ was observed in the crystal structure of ring-opened cephalexin bound to NDM-1.⁹ Thus, both N₃ and C₅ are identified as the likely proton acceptors during **EI** \rightarrow **EP** reaction. The factors controlling the protonation mechanism are yet to be scrutinized.

Asp124 bound to Zn2 was proposed to get protonated during the nucleophilic attack of the bridging hydroxyl group in NDM-1^{25,32} and other MBLs.^{27,28} Thus the protonated Asp124

formed after the nucleophilic attack could act as the proton donor.³⁶ However, detailed mutational studies indicate that Asp124 is not likely to be involved in the protonation of the intermediate.^{16,36,37} The same conclusion was also arrived by the QM/MM MD study of meropenem hydrolysis by NDM-1.³² The bridging hydroxyl group was proposed as the proton donor by Zhang and Hao based on the crystal structure of ampicillin complexed with NDM-1.¹⁰ Observation of water or hydroxyl group bound to the Zn ions in the crystal structures of the reaction intermediates¹² also hints that protonation might occur from the dissociation of the bulk water coordinating to the Zn site during the hydrolysis reaction. This mechanism was also supported by the previous QM/MM MD simulation, where a bulk water coordinates to Zn1 in the **EI** structure, which subsequently dissociate to protonate N₃.³²

Formation of anionic intermediate is also reported based on various spectroscopic data for di-Zn MBLs^{13,18,21,23,24,38} and further supported by QM/MM simulations.^{25,27,28,30,32} X-ray structures of di-Zn MBLs with ring-opened drug molecules have N₃-Zn2 coordination, thus these structures are likely to be the “trapped” **EI** intermediate state.^{9,10,12,18,39,40} Spectroscopic and kinetic data of NDM-1 catalyzed hydrolysis of chromacef and nitrocefin suggest that the rate constant for **EI** → **EP** (k_3) is nearly 10 times smaller than **ES** → **EI** (k_2) hinting on the accumulation of the anionic intermediate.^{23,24} Based on the kinetic parameters derived from these experiments, it was concluded that the rate determining step is the protonation of the anionic intermediate (i.e. **EI** → **EP**). This is also consistent with the kinetic studies where solvent isotope effect was observed in the hydrolysis of various drug molecules by di-Zn MBLs.^{13,16,41} Previous QM/MM study also agrees with the formation of stable anionic intermediate, where the negative charge of β -lactam N is stabilized by Zn2.³²

The predicted mechanism from QM/MM MD simulation is composed of a water diffusion towards the active site after the formation of the **EI** complex.³² The diffused water molecule coordinates with Zn1, which subsequently acts as the proton donor. However, coordination of a bulk water molecule is anticipated to be a slow process in the complexed structure,

and thus an alternative mechanism was proposed for di-Zn MBLs by Vila and co-workers where the apoenzyme active site is considered to be composed of Zn₂ coordinated with a additional water molecule (W2).³³ According to this mechanism, the proton transfer to the anionic intermediate occurs directly from W2. Klein and co-workers have carried out QM/MM MD simulation of CCrA catalyzed hydrolysis using this active site model and found that accumulation of anionic species doesn't occur since proton transfer to N₃ occurs spontaneous with the formation of **EI**.²⁶ Based on this a pre-coordinated water model can be excluded as accumulation of anionic species is observed in various experiments. Further, crystallographic structures were found without any bulk water molecules coordinated at the Zn sites in the trapped reaction intermediate states.¹²

In this work, we investigate various mechanistic routes for cephalixin and meropenem hydrolysis catalyzed by NDM-1. Primarily, we address the question of N₃ protonation versus C₅ protonation. First principle density functional theory (DFT) based QM/MM Car-Parrinello MD⁴² combined with conventional^{43,44} and the recently developed well-sliced metadynamics⁴⁵ approaches are used here for simulating chemical reactions and to obtain free energy barriers.

Methods and Models

We followed a three step simulation strategy in this work. At first, we carried out MM force-field MD simulations of the fully solvated protein-drug complexes **ES** of cephalixin and meropenem. This was followed by DFT based QM/MM MD simulations to further equilibrate these systems. Finally, taking the equilibrated structures, we performed QM/MM metadynamics or well-sliced metadynamics simulations to model chemical reactions. The reaction mechanism and free energy barriers of all elementary steps are obtained from these simulations.

Henry-Michaelis complexes of NDM-1 with cephalixin and meropenem were built from

the crystal structures of NDM-1 complex with hydrolyzed drug molecules, PDB IDs 4RL2⁹ and 4EYL,¹² respectively. Restrained Electrostatic Potential (RESP) derived point charges of the drug molecules were computed using the R.E.D tools⁴⁶ (see SI) and the potentials for the drug molecules were described by the GAFF force-field.⁴⁷ The protonation states for all the ionizable residues of the protein were set to that correspond to pH= 7. We considered Asp124 in the deprotonated form, as found in our earlier study.⁴⁸ All the crystal structure water molecules were retained while building the initial structure. Two Zn atoms are bridged by a hydroxyl, and the Zn1 site is coordinated with His120, His122, and His189, whereas the Zn2 site is bound to Asp124, Cys208, and His250; see SI Figure S1. Zn-ligand coordination was modeled following the work of Suarez *et al.*³¹ While modeling the cephalexin-NDM-1 complex three Na⁺ ions were added to neutralize the whole system which was solvated with 8914 water molecules in a periodic box of dimensions 66×75×76 Å³. In order to model the solvated meropenem-NDM-1 complex, we added four Na⁺ ions to the system containing the protein in a periodic box of 70×68×72 Å³ containing 7990 water molecules. The parm99⁴⁹ version of the AMBER force field was used to model the protein. MM water molecules were treated using the TIP3P⁵⁰ force field. The particle-mesh Ewald method⁵¹ was employed to compute the long range electrostatics, and a non-bonded interaction cutoff of 15 Å was used.

Sander module of the AMBER program package was used to perform MM MD simulations.⁵² These MD simulations were carried out with a time step of 1 fs. All the atoms in the system, including the solvent molecules were relaxed during the MD simulations. We performed nearly 2 ns *NPT* simulation at 1 atm and 300 K using Berendsen barostat⁵³ and Langevin thermostat⁵⁴ in order to obtain the equilibrium density. With the equilibrated cells, we carried out 10 ns of *NVT* MD simulations. These simulations were carried out till the RMSD fluctuations of the backbone and the active sites have converged satisfactorily; see SI Figure S3.

Hybrid QM/MM simulations^{42,55-57} of the equilibrated structures obtained from the MM simulations were performed using the CPMD/GROMOS interface, as available in the CPMD

package.⁵⁸ In these simulations, the whole drug molecule, two Zn ions, the embedded hydroxide and the coordinated side chains of His120, His122, Asp124, His189, Cys208, His250, were treated quantum mechanically; see SI Figure S2. Additionally, one water molecule (W2) was also treated quantum mechanically when modeling **EI1** \rightarrow **EI2** reaction, while the side chain of Lys211 as well as two water molecules (W3 and W4) were described quantum mechanically for modeling **EI1** \rightarrow **EI2'** reaction; see SI Figure S4(b). We used capping hydrogen atoms to saturate the dangling chemical bonds of the QM part. Capping hydrogen atoms were placed between the C_β - C_γ bonds in His120, His122, His189 and His250, between the C_α - C_β bonds in Asp124 and Cys208 and between C_δ - C_ϵ bond in Lys211 (SI Figure S2). A cubic QM box with a side length of 27.5 Å was used, and the QM subsystems were treated at the DFT level using the PBE⁵⁹ density functional and ultra soft pseudopotentials were used to describe the core-potentials.⁶⁰ Plane wave basis set with a plane wave cutoff of 25 Ry was used in these calculations. The QM/MM electrostatic coupling was treated using the scheme by Laio *et al.*⁴² The QM/MM MD runs were carried out using the Car-Parrinello method with a time step of 0.125 fs and a fictitious mass of 700 a.u. for the orbital degrees of freedom.^{57,61} The nuclear and the orbital degrees of freedom were thermostated using Nosé-Hoover chains thermostats.⁶² Ionic temperature in the MD simulations was set to 300 K. We carried out *NVT* QM/MM MD simulations for nearly 10 ps for both the systems, before starting metadynamics simulations.

In order to accelerate the sampling of chemical reactions, thus to obtain reaction mechanism and free energy barriers, we used the metadynamics method.^{43,63-66} By applying dynamically grown biasing potentials, metadynamics technique enhances the sampling of a selected set of collective variables (CVs) that are relevant for a chemical reaction. We employed the extended Lagrangian variant of metadynamics,⁴⁴ and the details of the metadynamics simulation setup and the choice of CVs for various elementary steps of the hydrolysis reaction can be found in SI Section 8. We also used the well-sliced metadynamics approach,⁴⁵ for exploring broad and unbound free energy surfaces by a combination of umbrella sampling

and metadynamics techniques. Initial structures of metadynamics simulations were taken from the equilibrated structures obtained from QM/MM *NVT* runs.

The transition state for the step **ES**→**EI** was obtained through committer analysis⁶⁷ ; see Section SI 10. Accuracy of the free energy estimates, considering the typical errors due to metadynamics and the density functional is about $(W+1)$ kcal mol⁻¹, where W is the height of the Gaussian potentials used in metadynamics; see Section SI 11.

Results and Discussion

In order to study the hydrolysis of cephalexin, first we equilibrated the **ES** structure using MM, QM/MM MD simulations (see SI Figure S1 and SI Section 4) and then we explored five different reaction pathways using a series of metadynamics simulations (see SI Table S3).

The **Path 1**, which we investigated first, is **ES** → **EI1** → **EI2** → **EI3** → **EP**; see Figure 2. This pathway is identical to that we proposed in our earlier study on meropenem hydrolysis.³² The elementary reaction steps were explored using independent metadynamics simulations, and based on which, free energy barriers for the elementary steps were computed; see Figure 3. The first step **ES** → **EI1** involves the ring-opening reaction where the bridging O_{W1} attacks C₂. Most importantly, in the **ES** structure, Zn1 and Zn2 are only weakly coordinated to O₁ and O₉, respectively, while these interactions strengthen as the O_{W1}···Zn2 coordination interaction is weakened. Hydrogen bonding interaction between H_{W1} and Asp124:O_{δ1} is favorably orienting W1 for the nucleophilic attack on C₂. Subsequently, O_{W1} attacks C₂, and C₂-N₃ bond is cleaved. Almost simultaneous with C₂-N₃ bond breakage, we observed coordination of N₃ to Zn2, Zn2-Asp124:O_{δ2} bond dissociation, and H_{W1} transfer from O_{W1} to Asp124:O_{δ1}; see SI Figure S20. It is interesting to note that these processes were occurring almost simultaneously near the transition state. For further verification we characterized the transition state for **ES** → **EI1** reaction through committor analysis and the structure of the transition state is shown in SI Figure S8(a). In the transi-

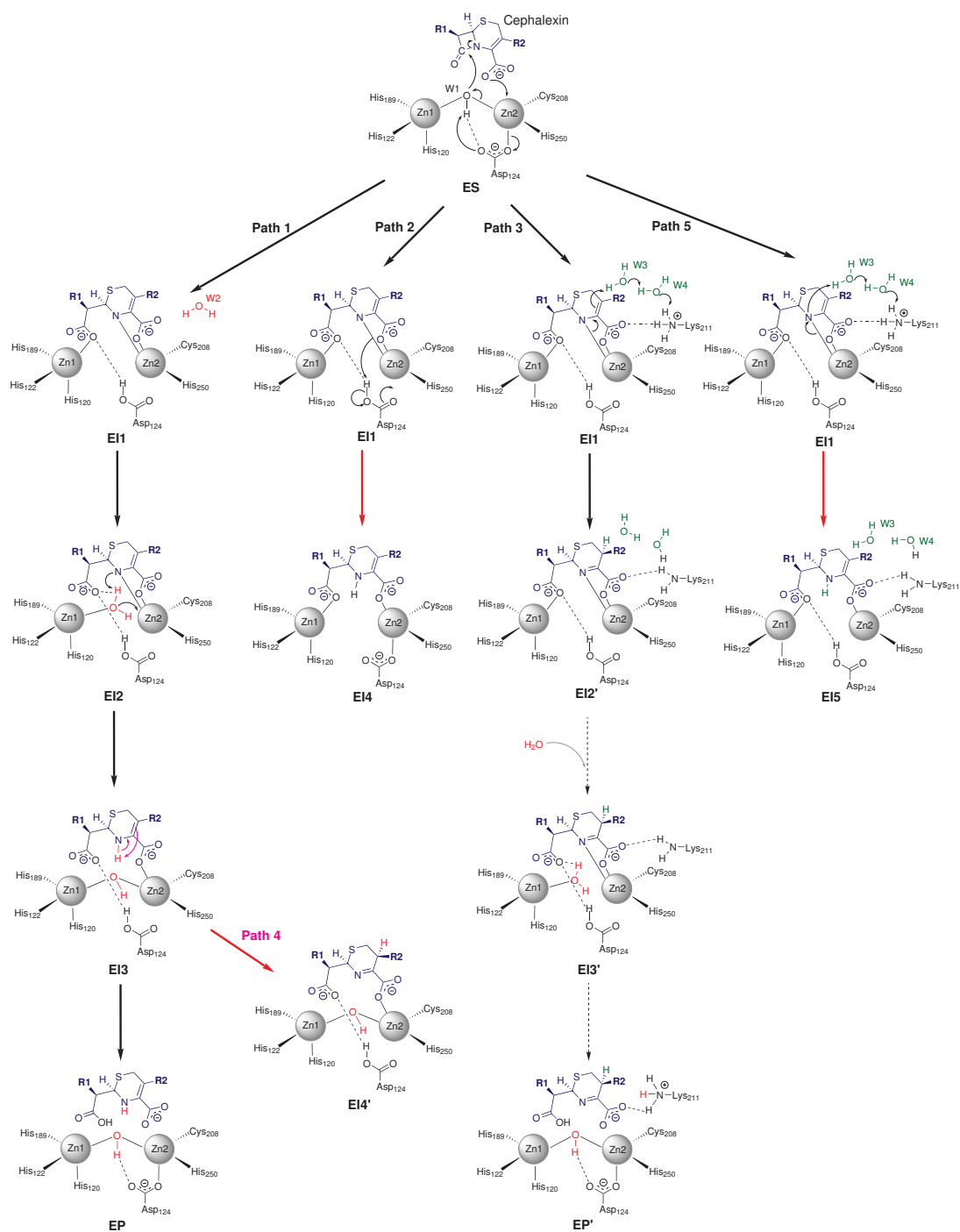


Figure 2: Mechanistic paths of cephalosporin hydrolysis by NDM-1 explored in our QM/MM-simulations. Red arrows indicate energetically unfavorable reaction pathways. Dotted arrows are hypothesized steps on the basis of our simulation. See SI Figure S23 for the mechanistic routes investigated for meropenem hydrolysis.

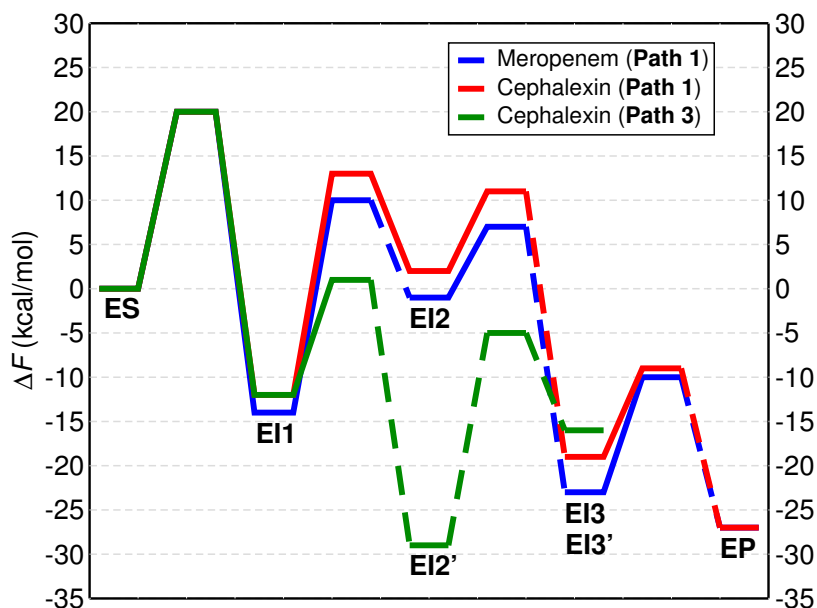


Figure 3: Free energy profile for the various pathways for meropenem and cephalixin hydrolysis. Solid lines are computed from our calculations while dotted lines are tentative and not determined from our computations.

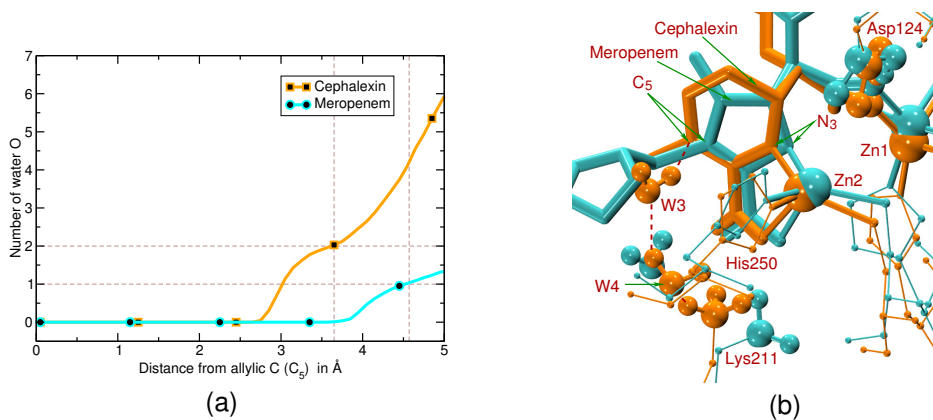


Figure 4: (a) The number of water molecules surrounding to the allylic C of β -lactam N (C_5) during *NVT* QM/MM simulation of the **EI1** is calculated by integrating radial distribution function ($g(r)$) of all water oxygen atoms from C_5 . (b) Overlapped **EI1** structures after QM/MM equilibration for the case of meropenem (cyan) and cephalixin (orange).

tion state, C_2-N_3 distance is 1.58 Å, and $O_{W1}-C_2$ distance is 1.51 Å. Of great importance, we notice that H_{W1} is delocalized between O_{W1} and Asp124: $O_{\delta 1}$ in the transition state structure. According to the computed free energy profile in Figure 3, we find that the free energy barrier for **ES**→**EI1** (20 kcal mol⁻¹; see SI Figure S9) was found to be smaller than the reverse step **EI1**→**ES** (32 kcal mol⁻¹; see SI Figure S10)

In the **EI1** structure, a bulk water molecule (W2) is located near the hydrophilic pocket consisting of the C_4 carboxylate, Lys211, and backbone amide hydrogen of Asn220; see SI Figure S4(b). **EI1** → **EI2** composes of diffusion of W2 (which was treated quantum mechanically in this simulation), followed by coordination to Zn1 and the associated decoordination of O_1 and O_{W1} from Zn1; see SI Figure S5. The free energy barriers for **EI1** → **EI2** and for the reverse step were computed as 25 kcal mol⁻¹ (SI Figure S11) and 11 kcal mol⁻¹ (SI Figure S12), respectively.

EI2 → **EI3** is the N_3 protonation step. While modeling this step, we sampled two protonation pathways in the same simulation: (a) protonation by the transfer of H_{W1} protons, which are coordinated to Asp124: $O_{\delta 1}$ and O_{W1} ; (b) protonation by the transfer of H_{W2} protons of the W2 water molecule coordinated to Zn1. However, we have found that transfer of H_{W2} to N_3 is the preferred route for N_3 protonation. The free energy barrier for this reaction was computed as 9 kcal mol⁻¹ (SI Figure S13). With the formation of **EI3**, the hydroxyl bridge is reformed as in the **ES** structure, yet Asp124: $O_{\delta 1}$ is protonated and Asp124: $O_{\delta 2}$ is weakly bound to the Zn2 site. Thus we modeled **EI3** → **EP**, where we sampled the coordination of Asp124: $O_{\delta 2}$ and decoordination of O_9 from the Zn2 site. Here we observed the product (**EP**) formation, where the H_{W1} is first transferred to O_{W1} from Asp124: $O_{\delta 1}$, and Asp124: $O_{\delta 2}$ coordinates to Zn2. This process is also synchronous with the decoordination of O_9 from Zn2. The free energy barrier for this reaction was computed as 10 kcal mol⁻¹ (SI Figure S14).

Having determined the mechanism and free energy profile along **Path 1**, we modeled the reaction along **Path 2**, where the reaction proceeds through **ES** → **EI1** → **EI4**; see Figure 2.

Here, we explored the possibility of protonation of N₃ in **EI1**, before the water diffusion to the active site, through a direct proton transfer from W1 to N₃. This is motivated by the work of Zhang and Hao, who proposed this mechanism based on the close distance between O_{W1} and N₃ in the crystal structure PDB ID 3Q6X.¹⁰ In our simulation, we observed the proton transfer to N₃ from Asp124:O_{δ1}. The free energy barrier for this reaction was computed to be 36 kcal mol⁻¹ (SI Figure S15). Thus it is clear that **Path 1** is preferred over **Path 2**; see Figure 3).

Subsequently, we explored **ES** → **EI1** → **EI2'** → **EI3'** → **EP**, i. e. **Path 3**; see Figure 2. Along this pathway, we investigated the possibility of C₅ protonation. On our careful analysis of the equilibrated **EI1** structure, we observed that a water molecule (W3) is in the vicinity of C₅. Interestingly, W3 is hydrogen bonded to another water molecule (W4), which in turn is hydrogen bonded to protonated Lys211; see SI Figure S4(b). Thus we explored proton transfer to C₅ from Lys211 through W3 and W4. Tautomerization of the double bond from C₄-C₅ to C₄-N₃ in the six membered ring should also take place during this reaction. We successfully simulated this reaction, and found that the free energy barrier for **EI1** → **EI2'** is 13 kcal mol⁻¹ (SI Figures S16 and S22). Free energy profiles for **Path 1** and **Path 3** (Figure 3) indicate that cephalixin hydrolysis proceeds preferably through C₅ protonation along **Path 3**, rather than via N₃ protonation along **Path 1**, since the former has a smaller free energy barrier for protonation. We hypothesize that, **EI2'** further results in **EP'** after the coordination of a bulk water molecule to the active site as in **EI1** → **EI2** along **Path 1**. The crystal structures of the hydrolyzed cephalixin bound to NDM-1 reported by Feng *et al.*⁹ where C₅ is in tetrahedral coordination also embeds an oxygen atom between the two Zn ions. On the other hand, the observation of C₅ protonation in Tioni *et al.*¹⁸ experiment is anticipated to be due to tautomerization of the product after the release, instead of protonation by Lys211 since their experiments were conducted with cephalosporins having large R2 groups.

As next, we investigated the 1,3-proton shift occurring from N₃ to C₅ in **EI3**, i.e. **ES** →

EI1 \rightarrow **EI2** \rightarrow **EI3** \rightarrow **EI4'** (**Path 4**); see Figure 2. In that simulation, we explicitly sampled the tautomerization of double bond in the six membered ring of the drug molecule, however, no 1,3-proton shift was observed even after applying a bias potential of 30 kcal mol⁻¹ (SI Figure S18). Thus, we excluded the possibility that **Path 4** is a preferred reaction pathway.

Another pathway which we studied was **Path 5**, i.e. **ES** \rightarrow **EI1** \rightarrow **EI5**, where proton transfer from the protonated Lys211 occurs to N₃ (instead of C₅ as in **Path 3**), through W3 and W4 water molecules; see Figure 2. However, this reaction was not observed, even after applying a bias potential of 30 kcal mol⁻¹ (SI Figure S19). Thus we conclude that **Path 3** is the preferred protonation pathway compared to **Path 5**.

As next we revisited meropenem hydrolysis mechanism which we carried in our previous work.³² In particular, we performed computations of all elementary steps along **Path 1** and **Path 3** using the same procedures used for studying cephalixin hydrolysis, as before. see Figure 3 and SI Section 17. Along **Path 1** the free energy profile has qualitatively the same feature as that for cephalixin. The free energy barrier for **ES** \rightarrow **EI1** along **Path 1** was also computed to be identical (20 kcal mol⁻¹) for both cephalixin and meropenem. However, in the **EI1** structure corresponding to meropenem, a water chain connecting Lys211 to C₅ was absent unlike in the case of cephalixin. Thus, we exclude the possibility of **Path 3** in the case of meropenem. The origin of this difference between meropenem and cephalixin could be ascribed to the differences in the R2 groups of these drug molecules. Clearly, cephalixin has a small R2 group compared to that for meropenem; see Figure 1. Our analysis indicates that the bulky R2 group of meropenem could result in large steric effect such that it blocks the formation of stable water chain connecting Lys211 and C₅. This is evident from Figure 4(a), where the number of water molecules surrounding the allylic C₅ atom is plotted, obtained by integrating the corresponding radial distribution function computed along the canonical ensemble trajectory of the **EI1** structure. In the case of cephalixin, there are two water molecules within 4 Å of C₅, while this is nearly zero for meropenem. The

overlapped structures of **EI1** with meropenem and cephalexin in Figure 4(b), also indicates that position of W3 in cephalixin is occupied by the five membered ring part of the R2 group of meropenem. Thus, our study leads to the conclusion that depending on the bulkiness of the R2 group, the protonation mechanism could change.

We compared the equilibrated structures of the intermediates observed along **Path 1** and **Path 3** with the available X-ray structures; see SI Section 9. Strikingly, the crystal structure of NDM-1 with ring-opened cephalixin (PDB ID 4RL2⁹) has significant similarity with the **EI2'** structure; see SI Figure S7 and SI Table S5. In particular, we find that the orientation of the proton at the C₅ position is identical with the crystal structure. Thus, the crystal structure is more likely to be **EI3'** state, where Zn1 has a bound water molecule (via **EI2' → EI3'**). This is a strong support for the proposed mechanism of protonation of C₅ from Lys211. Additionally, the intermediate **EI1** found in our study along the meropenem hydrolysis pathway matches very well with the crystal structure PDB ID 4EYL;¹² see SI Figure S7 and SI Table S6. It is worth noting that no water molecules are bound to Zn1 and Zn2 in this crystal structure, thus confirming our proposed mechanism that the coordination of a bulk water molecule occurs after the formation of **EI1**. The crystal structure of NDM-1 with ampicillin (PDB ID: 3Q6X¹⁰) having Zn1 bound water is likely to represent either **EI2** or **EI3**. Such excellent agreements with the crystal structural data support the proposed reaction pathways in our study.

If reaction pathways **Path 1** and **Path 3** is casted to the following enzymatic reaction model



then

$$k_{\text{cat}} = \frac{k_2 k_3}{k_2 + k_3} . \tag{1}$$

In this model, we consider that k_3 is the effective rate constant for the decay of **EI1**, which includes proton transfer to the substrate, water coordination to the active site, and product decoordination. Since **EI1** \rightarrow **E** + **P** involves water coordination from the bulk, and the barrier for this process is higher than that for the other elementary steps, we arrive at $k_{\text{cat}} \approx k_3$. In the kinetic experiments by Yang *et al.*,^{23,24} the authors have found that $k_{\text{cat}} \approx k_3$ for NDM-1 catalyzed hydrolysis of nitrocefin and chromacef molecules. Thus the experimental data is in line with our studies. Further, both their experiment and our proposed mechanism supports the accumulation of anionic intermediates. k_{cat} values measured for various cephalosporins and carbapenems catalyzed by NDM-1 and BcII enzymes do not vary much (which is only an order of magnitude).^{3,68} This is consistent with our conclusion that $k_{\text{cat}} \approx k_3$. We also predict that solvent isotope effects will influence k_{cat} as **EI1** \rightarrow **E**+**P** involves water coordination and deprotonation. This is consistent with the observation of solvent isotope effects in the experiments by Vila and co-workers.¹⁶

Conclusion

We find that the detailed mechanism of hydrolysis by the two drug molecules, namely cephalexin and meropenem, are different. The ring-opening mechanism and the corresponding free energy barriers are identical for both the drug molecules. However, the mechanism of proton transfer steps for the two drug molecules differ. Protonation of the ring-opened substrate could occur in two different ways. In one case, proton transfer occurs to the β -lactam nitrogen of the ring-opened intermediate by a water molecule which diffuses into the active site after the ring-opening reaction. Along the other route, proton transfer occurs from Lys211 to C₅ through a chain of two water molecules. The latter mechanism would take place when the drug molecules contain small R2 group as in the case of cephalexin, while the former mechanism is active for drug molecules such as meropenem having a larger R2 group. Observation of different protonation pathways also agree well with the crystal structures of

the reaction intermediates involving cephalexin and meropenem. We conclude that $k_{\text{cat}} \approx k_3$ and thus is determined mostly by the water coordination reaction that occurs prior to the N_3 protonation in the case of nitrocefin, while it takes place after the C_5 protonation in the case of cephalexin. This is also in agreement with various experimental kinetic studies. The detailed mechanistic picture, especially the structural and energetic data, presented in this work brings new molecular understanding on the catalytic reactions by NDM-1 and we believe that these results will aid in the ongoing research towards developing novel drugs and inhibitors targeting NDM-1.

Acknowledgement

Authors are grateful to IIT Kanpur for availing the HPC facility and Department of Biotechnology, India, for funding this project. Authors also acknowledge the technical discussions with Dr. Ravi Tripathi and Ms. Shalini Awasthi. CKD thanks IIT Kanpur for his Ph.D. scholarship.

References

- (1) WHO, *Antimicrobial resistance: global report on surveillance 2014*; WHO Press, World Health Organization: Geneva, 2014; <http://www.who.int/drugresistance/documents/surveillancereport/en/> (accessed Oct 25, 2016).
- (2) The Review on antimicrobial resistance. Final report. <http://amr-review.org/Publications> (accessed Oct. 25, 2016).
- (3) Yong, D.; Toleman, M. A.; Giske, C. G.; Cho, H. S.; Sundman, K.; Lee, K.; Walsh, T. R. Characterization of a new metallo- β -lactamase gene, blaNDM-1, and a novel Ery-

- thromycin esterase gene carried on a unique genetic structure in *Klebsiella pneumoniae* sequence type 14 from India. *Antimicrob. Agents Chemother.* **2009**, *53*, 5046–5054.
- (4) Kumarasamy, K. K.; Toleman, M. A.; Walsh, T. R.; Bagaria, J.; Butt, F.; Balakrishnan, R.; Chaudhary, U.; Doumith, M.; Giske, C. G.; Irfan, S. et al. Emergence of a new antibiotic resistance mechanism in India, Pakistan, and the UK: a molecular, biological, and epidemiological study. *Lancet Infect. Dis.* **2010**, *10*, 597–602.
- (5) Nordmann, P.; Poirel, L.; Walsh, T. R.; Livermore, D. M. The emerging NDM carbapenemases. *Trends Microbiol.* **2011**, *19*, 588–595.
- (6) Bushnell, G.; Mitrani-Gold, F.; Mundy, L. M. Emergence of New Delhi metallo- β -lactamase type 1-producing Enterobacteriaceae and non-Enterobacteriaceae: global case detection and bacterial surveillance. *Int. J. Infect. Dis* **2013**, *17*, e325–e333.
- (7) Tada, T.; Shrestha, B.; Miyoshi-Akiyama, T.; Shimada, K.; Ohara, H.; Kirikae, T.; Pokhrel, B. M. NDM-12, a novel New Delhi metallo- β -lactamase variant from a carbapenem-resistant *Escherichia coli* clinical isolate in Nepal. *Antimicrob. Agents Chemother.* **2014**, *58*, 6302–6305.
- (8) Shrestha, B.; Tada, T.; Miyoshi-Akiyama, T.; Shimada, K.; Ohara, H.; Kirikae, T.; Pokhrel, B. M. Identification of a novel NDM variant, NDM-13, from a multidrug-resistant *Escherichia coli* clinical isolate in Nepal. *Antimicrob. Agents Chemother.* **2015**, *59*, 5847–5850.
- (9) Feng, H.; Ding, J.; Zhu, D.; Liu, X.; Xu, X.; Zhang, Y.; Zang, S.; Wang, D.; Liu, W. Structural and mechanistic insights into NDM-1 catalyzed hydrolysis of cephalosporins. *J. Am. Chem. Soc.* **2014**, *136*, 14694–14697.
- (10) Zhang, H.; Hao, Q. Crystal structure of NDM-1 reveals a common β -lactam hydrolysis mechanism. *FASEB J.* **2011**, *25*, 2574–2582.

- (11) Kim, Y.; Tesar, C.; Jedrzejczak, R.; Babnigg, J.; Mire, J.; Sacchettini, J.; Joachimiak, A. Structure of apo- and monometalated forms of NDM-1 – a highly potent carbapenem-hydrolyzing metallo- β -lactamase. *FASEB J.* **2013**, *27*, 1917–1927.
- (12) King, D. T.; Worrall, L. J.; Gruninger, R.; Strynadka, N. C. J. New Delhi metallo- β -lactamase: Structural insights into β -lactam recognition and inhibition. *J. Am. Chem. Soc.* **2012**, *134*, 11362–11365.
- (13) Wang, Z.; Fast, W.; ; Benkovic, S. J. Direct observation of an enzyme-bound intermediate in the catalytic cycle of the metallo- β -lactamase from *Bacteroides fragilis*. *J. Am. Chem. Soc.* **1998**, *120*, 10788–10789.
- (14) Rydzik, A. M.; Brem, J.; van Berkel, S. S.; Pfeffer, I.; Makena, A.; Claridge, T. D. W.; Schofield, C. J. Monitoring conformational changes in the NDM-1 metallo- β -lactamase by 19F NMR spectroscopy. *Angew. Chem. Int. Ed.* **2014**, *53*, 3129–3133.
- (15) Yamaguchi, Y.; Kuroki, T.; Yasuzawa, H.; Higashi, T.; Jin, W.; Kawanami, A.; Yamagata, Y.; Arakawa, Y.; Goto, M.; Kurosaki, H. Probing the role of Asp-120(81) of metallo- β -lactamase (IMP-1) by site-directed mutagenesis, kinetic studies, and x-ray crystallography. *J. Biol. Chem.* **2005**, *280*, 20824–20832.
- (16) Llarrull, L. I.; Fabiane, S. M.; Kowalski, J. M.; Bennett, B.; Sutton, B. J.; Vila, A. J. Asp-120 locates Zn²⁺ for optimal metallo- β -lactamase activity. *J. Biol. Chem.* **2007**, *282*, 18276–18285.
- (17) Rasia, R. M.; Vila, A. J. Structural determinants of substrate binding to *Bacillus cereus* metallo- β -lactamase. *J. Biol. Chem.* **2004**, *279*, 26046–26051.
- (18) Tioni, M. F.; Llarrull, L. I.; Poeylout-Palena, A. A.; Martí, M. A.; Saggiu, M.; Periyannan, G. R.; Mata, E. G.; Bennett, B.; Murgida, D. H.; Vila, A. J. Trapping and characterization of a reaction intermediate in carbapenem hydrolysis by *B. cereus* metallo- β -lactamase. *J. Am. Chem. Soc.* **2008**, *130*, 15852–15863.

- (19) Breece, R. M.; Hu, Z.; Bennett, B.; Crowder, M. W.; Tierney, D. L. Motion of the zinc Ions in catalysis by a dizinc metallo- β -lactamase. *J. Am. Chem. Soc.* **2009**, *131*, 11642–11643.
- (20) Hawk, M. J.; Breece, R. M.; Hajdin, C. E.; Bender, K. M.; Hu, Z.; Costello, A. L.; Bennett, B.; Tierney, D. L.; Crowder, M. W. Differential binding of Co(II) and Zn(II) to metallo- β -lactamase Bla2 from *Bacillus anthracis*. *J. Am. Chem. Soc.* **2009**, *131*, 10753–10762.
- (21) McManus-Munoz, S.; Crowder, M. W. Kinetic mechanism of metallo- β -lactamase L1 from *Stenotrophomonas maltophilia*. *Biochemistry* **1999**, *38*, 1547–1553.
- (22) Hu, Z.; Periyannan, G.; Bennett, B.; Crowder, M. W. Role of the Zn1 and Zn2 sites in Metallo- β -lactamase L1. *J. Am. Chem. Soc.* **2008**, *130*, 14207–14216.
- (23) Yang, H.; Aitha, M.; Hetrick, A. M.; Richmond, T. K.; Tierney, D. L.; Crowder, M. W. Mechanistic and spectroscopic studies of metallo- β -lactamase NDM-1. *Biochemistry* **2012**, *51*, 3839–3847.
- (24) Yang, H.; Aitha, M.; Marts, A. R.; Hetrick, A.; Bennett, B.; Crowder, M. W.; Tierney, D. L. Spectroscopic and mechanistic studies of heterodimetallic forms of metallo- β -lactamase NDM-1. *J. Am. Chem. Soc.* **2014**, *136*, 7273–7285.
- (25) Zheng, M.; Xu, D. New Delhi metallo- β -lactamase I: Substrate binding and catalytic mechanism. *J. Phys. Chem. B* **2013**, *117*, 11596–11607.
- (26) Peraro, M. D.; Vila, A. J.; Carloni, P.; Klein, M. L. Role of zinc content on the catalytic efficiency of B1 metallo β -lactamases. *J. Am. Chem. Soc.* **2007**, *129*, 2808–2816.
- (27) Park, H.; Brothers, E. N.; Jr., K. M. M. Hybrid QM/MM and DFT investigations of the catalytic mechanism and inhibition of the dinuclear zinc metallo- β -lactamase CcrA from *Bacteroides fragilis*. *J. Am. Chem. Soc.* **2005**, *127*, 4232–4241.

- (28) Xu, D.; Guo, H.; ; Cui, Q. Antibiotic deactivation by a dizinc β -lactamase: Mechanistic insights from QM/MM and DFT studies. *J. Am. Chem. Soc.* **2007**, *129*, 10814–10822.
- (29) Xu, D.; ; Guo, H.; Cui, Q. Antibiotic binding to dizinc β -lactamase L1 from *Stenotrophomonas maltophilia*: SCC-DFTB/CHARMM and DFT studies. *J. Phys. Chem. A* **2007**, *111*, 5630–5636.
- (30) Zhu, K.; Lu, J.; Liang, Z.; Kong, X.; Ye, F.; Jin, L.; Geng, H.; Chen, Y.; Zheng, M.; Jiang, H. et al. A quantum mechanics/molecular mechanics study on the hydrolysis mechanism of New Delhi metallo- β -lactamase-1. *J. Comput.-Aided Mol. Des.* **2013**, *27*, 247–256.
- (31) Suárez, D.; Brothers, E. N.; ; Kenneth M. Merz, J. Insights into the structure and dynamics of the dinuclear zinc β -lactamase site from *Bacteroides fragilis*. *Biochemistry* **2002**, *41*, 6615–6630.
- (32) Tripathi, R.; Nair, N. N. Mechanism of meropenem hydrolysis by New Delhi metallo β -lactamase. *ACS Catal.* **2015**, *5*, 2577–2586.
- (33) Meini, M.-R.; Llarrull, L. I.; Vila, A. J. Overcoming differences: The catalytic mechanism of metallo- β -lactamases. *FEBS Lett.* **2015**, *589*, 3419–3432.
- (34) Umayal, M.; Tamilselvi, A.; Mugesh, G. In *Prog. Inorg. Chem.*; Karlin, K. D., Ed.; John Wiley & Sons, Inc., 2012; Vol. 57; pp 395–443.
- (35) Palzkill, T. Metallo- β -lactamase structure and function. *Ann. N. Y. Acad. Sci.* **2013**, *1277*, 91–104.
- (36) Crisp, J.; Connors, R.; Garrity, J. D.; Carenbauer, A. L.; Crowder, M. W.; ; Spencer, J. Structural basis for the role of Asp-120 in metallo- β -lactamases. *Biochemistry* **2007**, *46*, 10664–10674.

- (37) Garrity, J. D.; Carenbauer, A. L.; Herron, L. R.; Crowder, M. W. Metal binding Asp-120 in metallo- β -lactamase L1 from *Stenotrophomonas maltophilia* plays a crucial role in catalysis. *J. Biol. Chem.* **2004**, *279*, 920–927.
- (38) Wang, Z.; Fast, W.; ; Benkovic, S. J. On the mechanism of the metallo- β -lactamase from *Bacteroides fragilis*. *Biochemistry* **1999**, *38*, 10013–10023.
- (39) Spencer, J.; Read, J.; Sessions, R. B.; Howell, S.; Blackburn, G. M.; Gamblin, S. J. Antibiotic recognition by binuclear metallo- β -lactamases revealed by x-ray crystallography. *J. Am. Chem. Soc.* **2005**, *127*, 14439–14444.
- (40) Garau, G.; Bebrone, C.; Anne, C.; Galleni, M.; J.-M. Frère.; Dideberg, O. A metallo- β -lactamase enzyme in action: crystal structures of the monozinc carbapenemase CphA and its complex with biapenem. *J. Mol. Biol.* **2005**, *345*, 785–795.
- (41) Bounaga, S.; Laws, A. P.; Galleni, M.; Page, M. I. The mechanism of catalysis and the inhibition of the *Bacillus cereus* zinc-dependent β -lactamase. *Biochem. J.* **1998**, *331*, 703–711.
- (42) Laio, A.; VandeVondele, J.; Rothlisberger, U. A Hamiltonian electrostatic coupling scheme for hybrid Car-Parrinello molecular dynamics simulations. *J. Chem. Phys.* **2002**, *116*, 6941–6947.
- (43) Laio, A.; Parrinello, M. Escaping free-energy minima. *Proc. Natl. Acad. Sci.* **2002**, *99*, 12562–6.
- (44) Iannuzzi, M.; Laio, A.; Parrinello, M. Efficient exploration of reactive potential energy surfaces using Car-Parrinello molecular dynamics. *Phys. Rev. Lett.* **2003**, *90*, 238302.
- (45) Awasthi, S.; Kapil, V.; Nair, N. N. Sampling free energy surfaces as slices by combining umbrella sampling and metadynamics. *J. Comp. Chem.* **2016**, *37*, 1413–1424.

- (46) Dupradeau, F.; Pigache, A.; Zaffran, T.; Savineau, C.; Lelong, R.; Grivel, N.; Lelong, D.; Rosanski, W.; Cieplak, P. The R.E.D. tools: advances in RESP and ESP charge derivation and force field library building. *Phys. Chem. Chem. Phys.* **2010**, *12*, 7821–7839.
- (47) Wang, J.; Wolf, R. M.; Caldwell, J. W.; Kollman, P. A.; Case, D. A. Development and testing of a general amber force field. *J. Comp. Chem.* **2004**, *25*, 1157–1174.
- (48) Tripathi, R. *Molecular mechanism of antibiotic resistance by class-C and New Delhi metallo β -lactamases: A QM/MM molecular dynamics study*; Doctoral dissertation, IIT Kanpur, Kanpur, India, August 2014; see also <http://172.28.64.70:8080/jspui/handle/123456789/14708> (accessed Oct 25, 2016).
- (49) Cheatham, T. E.; Cieplak, P.; Kollman, P. A. A modified version of the Cornell et al. force field with improved sugar pucker phases and helical repeat. *J. Biomol. Struct. Dyn.* **1999**, *16*, 845–862.
- (50) Jorgensen, W. L.; Chandrasekhar, J.; Madura, J. D.; Impey, R. W.; Klein, M. L. Comparison of simple potential functions for simulating liquid water. *J. Chem. Phys.* **1983**, *79*, 926–935.
- (51) Darden, T.; York, D.; Pedersen, L. Particle mesh Ewald: An Nlog(N) method for Ewald sums in large systems. *J. Phys. Chem.* **1993**, *98*, 10089–10092.
- (52) Case, D. A.; Cheatham, T. E.; Darden, T.; Gohlke, H.; Luo, R.; Merz, K. M.; Onufriev, A.; Simmerling, C.; Wang, B.; Woods, R. J. The amber biomolecular simulation programs. *J. Comp. Chem.* **2005**, *26*, 1668–1688.
- (53) Berendsen, H. J. C.; Postma, J. P. M.; van Gunsteren, W. F.; DiNola, A.; Haak, J. R. Molecular dynamics with coupling to an external bath. *J. Chem. Phys.* **1984**, *81*, 3684–3690.

- (54) Loncharich, R. J.; Brooks, B. R.; Pastor, R. W. Langevin dynamics of peptides: The frictional dependence of isomerization rates of N-acetylalanyl-N'-methylethylamide. *Biopolymers* **1992**, *32*, 523–535.
- (55) Warshel, A.; Levitt, M. Theoretical studies of enzymic reactions: Dielectric, electrostatic and steric stabilization of the carbonium ion in the reaction of lysozyme. *J. Mol. Biol.* **1976**, *103*, 227 – 249.
- (56) Carloni, P.; Rothlisberger, U.; Parrinello, M. The role and perspective of ab initio molecular dynamics in the study of biological systems. *Acc. Chem. Res.* **2002**, *35*, 455–464.
- (57) Marx, D.; Hutter, J. *Ab Initio Molecular Dynamics*; Cambridge University Press, 2009.
- (58) CPMD, J. Hutter et al., IBM Corp 1990-2004, MPI für Festkörperforschung Stuttgart 1997-2001, see also <http://www.cpmc.org>.
- (59) Perdew, J. P.; Chevary, J. A.; Vosko, S. H.; Jackson, K. A.; Pederson, M. R.; Singh, D. J.; Fiolhais, C. Atoms, molecules, solids, and surfaces: Applications of the generalized gradient approximation for exchange and correlation. *Phys. Rev. B* **1992**, *46*, 6671–6687.
- (60) Vanderbilt, D. Soft self-consistent pseudopotentials in a generalized eigenvalue formalism. *Phys. Rev. B* **1990**, *41*, 7892–7895.
- (61) Car, R.; Parrinello, M. Unified approach for molecular dynamics and density-functional theory. *Phys. Rev. Lett.* **1985**, *55*, 2471–2474.
- (62) Martyna, G. J.; Klein, M. L.; Tuckerman, M. Nosé-Hoover chains: The canonical ensemble via continuous dynamics. *J. Chem. Phys.* **1992**, *97*, 2635–2643.

- (63) Laio, A.; Gervasio, F. L. Metadynamics: a method to simulate rare events and reconstruct the free energy in biophysics, chemistry and material science. *Rep. Prog. Phys.* **2008**, *71*, 126601.
- (64) Ensing, B.; Vivo, M. D.; Liu, Z.; Moore, P.; ; Klein, M. L. Metadynamics as a tool for exploring free energy landscapes of chemical reactions. *Acc. Chem. Res.* **2006**, *39*, 73–81.
- (65) Barducci, A.; Bonomi, M.; Parrinello, M. Metadynamics. *Wiley Interdiscip. Rev. Comput. Mol. Sci.* **2011**, *1*, 826–843.
- (66) Valsson, O.; Tiwary, P.; Parrinello, M. Enhancing important fluctuations: Rare events and metadynamics from a conceptual viewpoint. *Annu. Rev. Phys. Chem.* **2016**, *67*, 159–184.
- (67) Dellago, C.; Bolhuis, P. G.; Csajka, F. S.; Chandler, D. Transition path sampling and the calculation of rate constants. *J. Chem. Phys.* **1998**, *108*.
- (68) Tomatis, P. E.; Rasia, R. M.; Segovia, L.; Vila, A. J. Mimicking natural evolution in metallo- β -lactamases through second-shell ligand mutations. *Proc. Natl. Acad. Sci.* **2005**, *102*, 13761–13766.